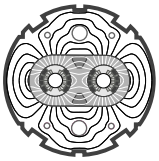

LHC Project Note 141

May 1998

bruening/tex/optics.v5.0/tdi.tex

Optics constraints imposed by the injection in IR2 and IR8

Oliver S. Brüning and J.B. Jeanneret SL/AP

Keywords: optics, injection, IR2, IR8

Summary

The aim of this note is to summarise the optics and acceptance constraints required by the injection elements in the two combined experimental and injection insertions at IR2 and IR8. These insertions are subject to special constraints imposed by the injection elements and the required protection of the super-conducting magnets in the triplet and the arc in case of a bad injection. Taking these constraints into account, this study gives upper limits for the allowed β functions inside the injection elements and the interaction region and the required vertical phase advance between MKI and TDI.

1 Introduction

The straight sections in IR2 and IR8 house the injection elements for Beam-1 and Beam-2 respectively as well as two experiments. During injection, the optics in both IR's must satisfy the safety requirements imposed by the beam injection while keeping the geometrical acceptance large enough to accommodate both beams in the common part of the ring with a beam separation of 10 σ. The cold elements of the machine must be protected against a bad injection. A graphite absorber (TDI) is installed down-stream from the injection kicker for this purpose and an optimum efficiency of the absorber requires a vertical phase advance of 90° between MKI and TDI. Separating the two beams at the IP during injection requires an orbit bump which extents from the MKI on the one side of the IP over the triplet quadrupoles to the Q5 quadrupole on the other side of the IP. The orbit bump reduces the acceptance of the injection elements and the magnets next to the IP. Taking these constraints into account, the following work gives upper limits for the tolerable β-function values inside the magnets of the two IR's.

An additional restriction comes from the requirement to accommodate the injected and circulating beam inside the injection kicker MKI and the Q4 quadrupole in case of a misfiring of the injection kicker. In the following, a misfiring of the injection kicker refers to both cases, a misfiring of the kicker with a circulating beam inside the chamber and the absence of the injection kick for the injected beam. The horizontal and vertical betatron functions at the injection kicker and Q4 must be small enough so that the elements can accommodate the

miskicked beams in both cases. The results of the following study apply to IR2 and IR8.

2 Geometrical Layout

The straight sections in IR2 and IR8 house the injection elements for Beam-1 and Beam-2 respectively as well as two experiments: ALICE, a heavy ion experiments in IP2 and LHC-B, a B-physics experiment for proton operation in IP8. Fig. 1 shows the corresponding layout left from IP2. The injection kicker MKI is located between the last two quadrupoles of the matching section next to the IP (Q4 and Q5) and the injection septum MSI is placed in the middle of the matching section between Q5 and Q6. The two quadrupoles left and right from the MKI are large aperture double-bore magnets with a half-aperture of $A = 31.5$ mm. The low-β triplet quadrupoles are single-bore large aperture magnets with a half-aperture of $A = 31.5$ mm. The quadrupoles inside the dispersion suppressor up to Q7 inclusive are normal arc double-bore quadrupoles with an aperture defined by the beam-screen (r22 mm-v18 mm). All other quadrupoles inside the matching section are double-bore magnets with a half-aperture of $A = 25.0$ mm [1].

At the IP the two beams cross from one channel to the other. The required orbit deflection is achieved by two pairs of separation/recombination dipoles. One pair (D1) has a single bore aperture and is located left and right from the low-β triplet of the IR. The second pair (D2) has a double bore aperture and is located next to the last quadrupole of the matching section (Q4 left and right from the IP).

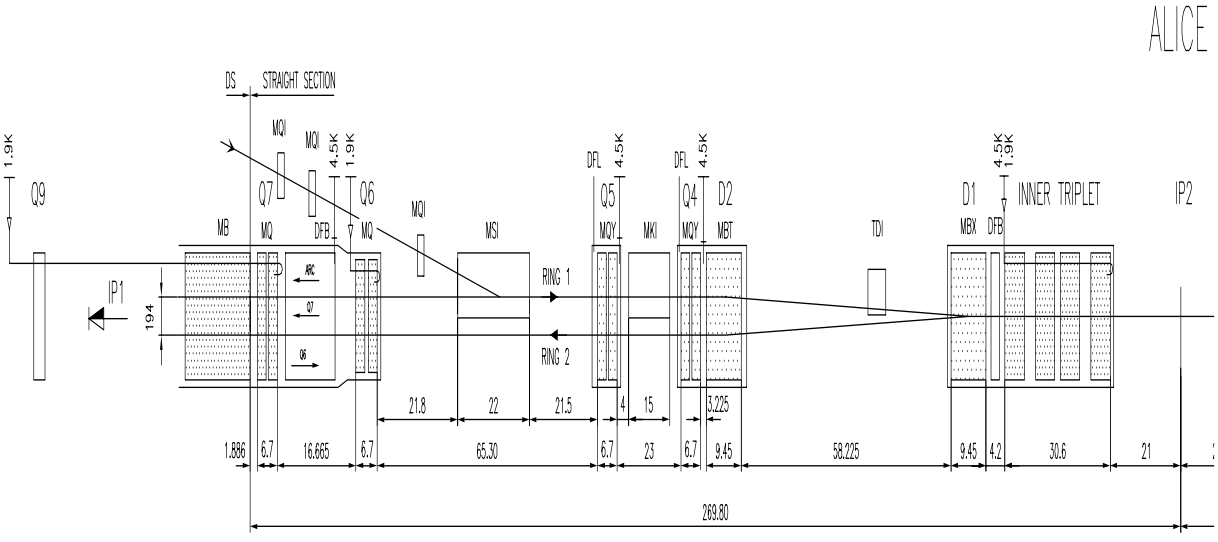

Figure 1: *The left side of IR2 with the injection line.*

In order to avoid an interaction of the two beams during injection and ramp the beams are separated in the common part of the interaction region by additional crossing-angle correctors. The crossing-angle correctors will be placed outside the common region of the two beams, allowing an independent steering of the two beams. The first crossing-angle corrector can

be placed next to Q4. The second crossing-angle corrector will be placed next to the Q5 quadrupole, leading to an orbit offset inside the MKI. The separation scheme at IR2 and IR8 foresees a crossing-angle in the vertical plane and a parallel separation in the horizontal plane. The left-hand side of Fig. 2 shows an example for the crossing-angle separation of the two beams during injection. The separation scheme has a vertical crossing-angle of ± 200 μrad and a horizontal separation of ± 2 mm.

3 Maximum β in the Injection Septum and Kicker

The injection septum MSI is a 21.8 m long object with a half-aperture of 20.0 mm. The injection kicker MKI is 15.0 m long and has a half-aperture of 19.0 mm. Fig. 1 shows the layout of the left side of the low-β insertion at IP2 with the injection elements. The MSI is located between Q6 and Q5 and kicks the injected beam in the horizontal plane towards the closed orbit of the circulating beam (the injected beam comes from the outside of the ring $\rightarrow$ positive deflection angle). The MKI kicks the injected beam in the vertical plane towards the closed orbit of the circulating beam (the injected beam comes from below the machine $\rightarrow$ negative deflection angle). In this section, we estimate the maximum allowed β-function values inside the injection elements. The analysis applies to both IR's: IR2 and IR8.

For the circulating beam, the maximum β-function values inside the MSI and MKI must be consistent with the acceptance limitation of the other magnets in the machine ($n_\sigma = 9.8$ [1]). The maximum β-function value for the circulating beam is given by

$$\sqrt{\beta_{max}} = \frac{\tilde{A}}{n_\sigma \cdot \sqrt{\epsilon} \cdot k_\beta}, \tag{1}$$

where $\tilde{A}$ is the remaining half aperture once the effect of the crossing-angle separation, the orbit errors and the alignment and mechanical tolerances of the element are taken into account. ϵ is the beam emittance at injection energy and k_β a coefficient measuring the effect of beta-beating due to gradient errors. The right-hand side of Fig. 2 shows the net beam offset inside a circular aperture with

$$\triangle x = k_\beta \cdot D_x \cdot \delta_p + \delta_{x,al} + \delta_{x,tol} + CO_x + \delta_{x,sep} \tag{2}$$

and

$$\triangle y = \delta_{y,al} + \delta_{y,tol} + CO_y + \delta_{y,sep} + \delta_{y,offset}. \tag{3}$$

D_x is the horizontal dispersion, δ_p the maximum momentum deviation, δ_{al} the alignment errors, CO the closed orbit offsets and δ_{tol} are the mechanical tolerances, δ_{sep} the maximum orbit offsets due to the crossing-angle separation and $\delta_{y,offset}$ the maximum trajectory deflection due to a misfiring of the injection kicker. Approximating the remaining aperture by the largest circle that has its origin at $(\triangle x, \triangle y)$ and still fits inside the initial aperture (see Fig. 2), the remaining aperture is given by

$$\tilde{A} = A - \sqrt{(\triangle x)^2 + (\triangle y)^2}, \tag{4}$$

[1] The smallest tolerable acceptance is determined by the aperture of the primary and secondary collimators. For the LHC we require a ratio of $n_2/n_1 = 7/6$ between the aperture of the primary and secondary collimators and the smallest tolerable radial magnet aperture is given by $n_r/n_1 = 1.4$ [1]. Requiring further $n_1 = 7$ for the primary collimators the radial aperture of the cold elements must be larger than $n_r = 9.8\sigma$.

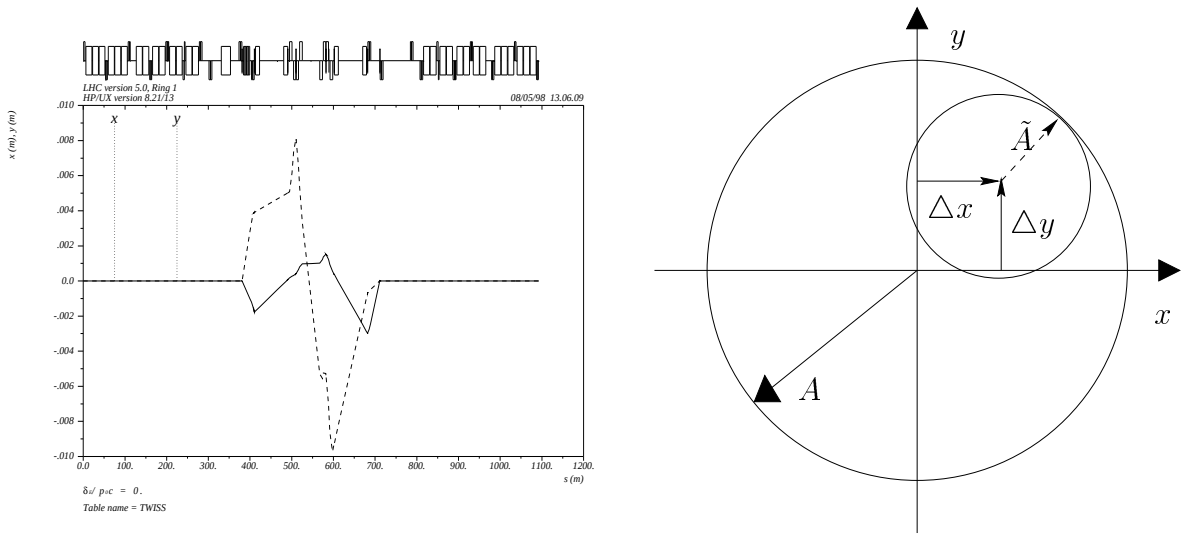

Figure 2:
Left: the crossing-angle orbit separation at the IP. The dotted line shows the vertical and the solid line the horizontal orbit. The scheme assumes a vertical half-crossing-angle of 210 μrad *and a horizontal parallel half-separation of 1 mm. Right: The net beam offset inside a circular aperture.*

where A is the half aperture of the chamber. The assumption of a circular aperture for $\tilde{A}$ gives a conservative estimate for the remaining aperture. Thus, the following discussion gives only a first estimate for the maximum allowed β-functions used for the optics matching. Once an optics solution is constructed one must still check the aperture with a program that incorporates the spatial extension of the secondary halo [1].

Table 1 lists the corresponding parameters common to all elements and Table 2 and 3 the parameters specific for the septum magnet and the injection kicker. The values for the

δ_p	CO_x [mm]	CO_y [mm]	ϵ	k_β
$1.0 \cdot 10^{-3}$	4.0	4.0	$7.82 \cdot 10^{-9}$	1.1

Table 1: *Acceptance parameters common to all elements. The beam emittance* ϵ *is based on an injection energy of 450 GeV.*

Element	A [mm]	D_x [m]	δ_{al} [mm]	δ_{tol} [mm]	δ_θ [mrad]
MSI	20.0	0.45	1.0	1.0	-
MKI	19.0	0.45	1.0	0.0	0.850

Table 2: *Acceptance parameters for the injection septum MSI and the injection kicker MKI.* δ_θ *specifies the maximum kick strength of the MKI at injection energy.*

horizontal dispersion represent a conservative upper bound for the dispersion.

Element	$\delta_{x,sep}$ [mm]	$\delta_{y,sep}$ [mm]	$\delta_{y,offset}(inj)$ [mm]	$\delta_{y,offset}(circ)$ [mm]
MSI	0.0	0.0	0.0	0.0
MKI-entrance	-0.5	1.0	-6.0	0.0
MKI-exit	-1.0	3.0	+6.0	-6.0

Table 3: *The assumed maximum orbit offsets due to the crossing-angle separation bump and the maximum trajectory offsets due to a misfiring of the injection kicker.* $\delta_{y,offset}(inj)$ *and* $\delta_{y,offset}(circ)$ *are the maximum trajectory deflections of the injected and the circulating beam due to a misfiring of the injection kicker respectively.*

3.1 Conditions for the circulating beam

Assuming a magnet aperture of $n_\sigma = 9.8$ and inserting the values from Table 1, 2 and 3 into Equations (4) and (1) one can estimate the maximum β-function values inside the MKI and the MSI. Table 4 lists the resulting β-function limits for the circulating beam.

Element	$\delta_{x,sep}$ [mm]	$\delta_{y,sep}$ [mm]	$\triangle x$ [mm]	$\triangle y$ [mm]	β_{max} [m]
MSI	0.0	0.0	6.5	6.0	150
MKI-entrance	-0.5	1.0	6.0	6.0	120
MKI-exit	-1.0	3.0	6.5	8.0	80

Table 4: β*-function limitations at the MSI and the MKI for the circulating beam.* $\delta_{max,sep,x}$ *and* $\delta_{max,sep,y}$ *are the upper limits for the crossing-angle orbits inside the magnets and* $\triangle x$ *and* $\triangle y$ *are the total beam offsets inside the magnets.*

3.2 Conditions for the miskicked circulating beam

Element	$\delta_{x,sep}$ [mm]	$\delta_{y,sep}$ [mm]	$\triangle x$ [mm]	$\triangle y$ [mm]	β_{max} [m]
MKI-exit	-1.0	3.0	6.5	8.0	160

Table 5: β*-function limitation at the exit of the MKI for the miskicked circulating beam.* $\delta_{max,sep,x}$ *and* $\delta_{max,sep,y}$ *are the upper limits for the crossing-angle orbits inside the MKI and* $\triangle x$ *and* $\triangle y$ *are the total beam offsets inside the kicker. We assumed a beam size of of 7* σ *(position of the primary collimator).*

The β-functions inside the kicker are further restricted by the requirement that the kicker must be able to house the miskicked beams. A misfiring of the MKI leads to an offset of -6 mm for the miskicked circulating beam at the exit of the kicker magnet. The miskicked beam will be absorbed by the TDI absorber down-stream of the injection kicker. In this case, we must only ensure that the beam fits through the aperture of the kicker and can relax the requirement of $n_\sigma = 9.8$ in Equation (1). For the circulating beam we assume a beam size of 7 σ (position of the primary collimator). A maximum β-function limit can be found if the vertical crossing-angle orbit is in the opposite direction from the deflection due to the miskick. In this case, the vertical crossing-angle orbit compensates part of the trajectory deflection due to the miskick. Table 5 shows the corresponding β-function limit at the exit of the MKI. It should be pointed

out at this point, that a smaller crossing-angle orbit will reduce the aperture for the miskicked circulating beam. Assuming, for example, a vanishing crossing-angle orbit in the vertical plane we get $\beta_{max}(kicker - out) = 80$ m ($\triangle x = 6.5$ mm, $\triangle y = 11$ mm).

3.3 Conditions for the miskicked injected beam

The injected beam has a vertical offset of -6 mm at the entrance of the kicker (Q5 side) and the miskicked injected beam an offset of +6 mm at the exit of the kicker. Assuming a beam size of 4 σ for the injected beam Table 6 shows the corresponding β-function limits in the MKI.

Element	$\delta_{x,sep}$ [mm]	$\delta_{y,sep}$ [mm]	$\triangle x$ [mm]	$\triangle y$ [mm]	β_{max} [m]
MKI-entrance	-0.5	1.0	6.0	12.0	200
MKI-exit	-1.0	3.0	6.5	14.0	80

Table 6: *β-function limitation at the MKI for the miskicked injected beam. $\delta_{max,sep,x}$ and $\delta_{max,sep,y}$ are the upper limits for the crossing-angle orbits inside the MKI and $\triangle x$ and $\triangle y$ are the total beam offsets inside the kicker. We assumed a beam size of of 4 σ for the injected beam.*

3.4 Summary of β limits in the MSI and MKI

Table 7 summarises the above results. All limits were obtained for a vertical crossing-angle orbit offset of +3 mm at the exit of the MKI. In this configuration, the vertical crossing-angle orbit inside the MKI improves the acceptance for the miskicked circulating beam by partially compensating the trajectory deflection in case of a misfiring of the MKI. In this case, the β-function limitation for the miskicked circulating beam (Table (4)) is larger than the limits found for the circulating beam and the miskicked injected beam (Tables (5) and (6)) suggesting that the overall acceptance inside the MKI could be increased by lowering the vertical crossing-angle orbit offset at the exit of the MKI. Thus, a vertical crossing-angle orbit offset of +3 mm at the exit of the MKI presents only an upper limit for the maximum orbit amplitude. Any value between 0.0 mm and +3.0 mm is compatible with the above β-function limits. The optimum vertical crossing-angle orbit offset at the exit of the MKI should be reevaluated using the aperture program described in [1] once an optical solution is constructed.

	MSI	MKI-entrance	MKI-exit
β_x [m]	150	120	80
β_y [m]	150	120	80
$\delta_{max,sep,y}$ [mm]	0.0	+1.0	+3.0
$\delta_{max,sep,x}$ [mm]	0.0	$\pm$0.5	$\pm$1.0

Table 7: *β-function limitations for the MSI and the MKI. $\delta_{max,sep,x}$ and $\delta_{max,sep,y}$ are the upper limits for the crossing-angle orbits inside the magnets. $\delta_{max,sep,y}$ must be positive and smaller than 3 mm at the exit of the MKI and $\delta_{max,sep,x}$ can take any value between -1.0 mm and +1.0 mm.*

4 Maximum β in Q4 and D2

Down-stream from the injection kicker is a large aperture double bore magnet Q4 and the separation/recombination dipole D2. In version 5.0, the Q4 magnet consists of two pieces, each 3.1 m long. The entrance of the Q4 magnet is approximately 11.5 m down-stream from the center of the MKI. The D2 dipole is 9.45 m long and the exit of the magnet is approximately 31.25 m down-stream from the center of the MKI. The miskicked beam must pass through the aperture of these two magnets before it can be absorbed by the TDI absorber. The Q4 magnet next to the MKI is defocusing and thus, reduces the vertical orbit offset in D2 for both beams, the miskicked circulating and the injected beam. The maximum vertical beam offset inside the Q4 magnet is given by

$$\delta_{y,offset(Q4)} = \delta_\theta \cdot \triangle L_{Q4}, \tag{5}$$

where $\triangle L_{Q4}$ is the distance of the Q4 magnet from the MKI. The maximum vertical beam offset inside the D2 magnet is given by

$$\delta_{y,offset(D2)} = \delta_\theta \cdot \triangle L_{D2} + \delta_{y,offset(Q4)} \cdot l_{Q4} \cdot \frac{0.2998}{p[GeV]} \cdot g_{Q4} \cdot (\triangle L_{D2} - \triangle L_{Q4}), \tag{6}$$

where $\triangle L_{D2}$ is the distance of the D2 magnet from the MKI, l_{Q4} and g_{q4} the length and strength of the Q4 quadrupole and p the beam momentum in GeV. Table 8 lists the corresponding trajectory offsets at the D2 magnet for different gradients of the Q4 quadrupole.

g_{Q4} [T/m]	-5.0	-7.5	-10.0	-12.5
K_{Q4}	$-3.33 \cdot 10^{-3}$	$-5.0 \cdot 10^{-3}$	$-6.66 \cdot 10^{-3}$	$-8.33 \cdot 10^{-3}$
$\delta_{y,offset}(D2)$ [mm]	23.1	21.4	19.6	17.9

Table 8: *Trajectory offsets at the D2 dipole for different gradients of the Q4 quadrupole in case of a misfiring of the MKI. g_{Q4} is the quadrupole gradient in T/m at injection and K_{Q4} the normalised quadrupole gradient (MAD units: $K = k/B\rho$).*

Following the same line of argumentation as in the previous section we estimate the maximum allowed β-function values inside these two magnets. Table 9 and 10 show the alignment parameters specific for the Q4 and D2 magnet respectively. The common parameters are given in Table 1. The vertical orbit offset $\delta_{y,offset}$ in D2 due to a misfiring of the MKI incorporates

A [mm]	D_x [m]	δ_{al} [mm]	δ_{tol} [mm]	$\delta_{x,sep}$ [mm]	$\delta_{y,sep}$ [mm]	$\delta_{y,offset}$ [mm]
31.5	0.45	0.6	1.0	$\pm$3.0	+4.0	15

Table 9: *Acceptance parameters for the Q4 quadrupole next to the MKI.*

A [mm]	D_x [m]	δ_{al} [mm]	δ_{tol} [mm]	$\delta_{x,sep}$ [mm]	$\delta_{y,sep}$ [mm]	$\delta_{y,offset}$ [mm]
37.0	0.45	0.6	1.6	$\pm$3.0	+4.0	19.6

Table 10: *Acceptance parameters for the D2 separation/recombination dipole next to the MKI. Here we assumed a quadrupole gradient of -10 T/m for the Q4 magnet.*

the additional kick from the off-center passage through the Q4 magnet. The data in Table 10 is based on a quadrupole strength of -10 T/m in Q4.

4.1 The miskicked injected beam

For the miskicked injected beam, $\delta_{y,sep}$ and $\delta_{y,offset}$ have the same sign and must be added. Assuming a beam size of 4 σ for the injected beam and inserting the values from Table 9 and 10 into Equation (1) one gets

$$\beta_{max}(Q4) = 180 \text{ m} \tag{7}$$

for the Q4 quadrupole ($\triangle x = 9.1$, $\triangle y = 24.6$). Table 11 shows the β-function limits at the D2 dipole for different gradients of the Q4 quadrupole.

g_{Q4} [T/m]	$\delta_{y,offset}(D2)$ [mm]	$\triangle x$	$\triangle y$	β
-5.0	23.1	9.7	33.3	35
-7.5	21.4	9.7	31.6	100
-10	19.6	9.7	29.8	210
-12.5	17.9	9.7	28.1	350

Table 11: *Trajectory offsets at the D2 dipole and the corresponding β-function limits for the miskicked injected beam at the D2 dipole for different gradients of the Q4 quadrupole.*

For Q4 gradients smaller than -7.5 T/m the constraints at the D2 dipole are weaker than those imposed by the injection kicker. For Q4 gradients larger than -7.5 T/m the β-function limits imposed by the D2 dipole are stronger than those imposed by the MKI. Thus, the absolute value of the Q4 gradient should be larger than 7.5 T/m during injection.

4.2 The miskicked circulating beam

For the miskicked circulating beam, $\delta_{y,sep}$ and $\delta_{y,offset}$ have opposite signs and must be subtracted. Assuming a beam size of 7 σ for the circulating beam and inserting again the values from Table 9 into Equation (1) one gets

$$\beta_{max}(Q4) = 340 \text{ m} \tag{8}$$

for the miskicked circulating beam inside the Q4 quadrupole ($\triangle x = 9.1$, $\triangle y = 16.6$). Table 12 shows the β-function limits at the D2 dipole for different gradients of the Q4 quadrupole. All limits are larger than those imposed by the MKI (see Table 7).

g_{Q4} [T/m]	$\delta_{y,offset}(D2)$ [mm]	$\triangle x$	$\triangle y$	β
-5.0	23.1	9.7	25.3	210
-7.5	21.4	9.7	23.6	280
-10	19.6	9.7	21.8	370
-12.5	17.9	9.7	20.1	460

Table 12: *Trajectory offsets at the D2 dipole and the corresponding β-function limits for the miskicked circulating beam at the D2 dipole for different gradients of the Q4 quadrupole.*

4.3 Summary

For Q4 quadrupole gradients smaller than -7.5 T/m the β-function limits imposed by the Q4 quadrupole and the D2 dipole are larger than the limits coming from the MKI. Because both magnets follow right after the MKI the β-functions can not be much different from the values at the MKI and fulfilling the β-function limits in Table 7 at the MKI also satisfies the aperture constraints at Q4 and D2. Thus, in order to avoid additional limits for the β-functions, the Q4 quadrupole gradients must be smaller than -7.5 T/m.

5 β-Function Limit in the Low-β Triplet

Assuming a maximum vertical crossing-angle of ± 200 μrad and neglecting the orbit kicks due to the offset in the low-β triplets, the maximum vertical beam separation inside the triplet magnets is given by

$$\delta_{y,sep} = \pm 200 \ \mu\text{rad} \cdot \triangle L, \tag{9}$$

where $\triangle L$ is the distance of the magnet from the interaction point. In the horizontal plane we assume a separation of ± 2 mm. Table 13 shows the corresponding parameters for D1 and the triplet magnets in IR2 (the maximum β-function and orbit occurs at the center of Q2 $\rightarrow$ the β-function limit for the D1 magnet given below is a conservative estimate). The parameters for the mechanical tolerances and alignment errors are taken from [1]. In all cases, we assume a maximum horizontal and vertical orbit error of $CO = 4$ mm and a required aperture of $n_\sigma = 9.8$ for the circulating beam.

Magnet	A [mm]	$\triangle L$	$\delta_{x,sep}$ [mm]	$\delta_{y,sep}$ [mm]	δ_{al} [mm]	δ_{tol} [mm]	β_{max}
D1	37.0	65.25	2.0	13.0	1.6	0.6	286.0
Q2	31.5	36.3	2.0	7.3	1.0	0.6	300.0

Table 13: *Tolerances, beam separations and corresponding β-function limits inside the D1 and the low-β triplet magnets. In all cases, we assume a maximum horizontal and vertical orbit error of $CO = 4$ mm.*

6 TDI Absorber

In order to protect the low-β triplet and the following arc-magnets in case of a faulty injection a graphite absorber (TDI) in front of the low-β triplet is foreseen. The required aperture of the TDI absorber was given in [2] assuming a point like beam. In the following, we give a similar analysis, taking into account the spatial extension of the beam and discussing different failure modes for the injection.

The injection error and the efficiency of the TDI absorber can be best analysed by looking at the normalised phase space. The vertical normalised coordinates are defined by

$$Y = \frac{y}{\sigma_y}; \quad Y' = \frac{\alpha_y \cdot y + \beta_y \cdot y'}{\sigma_y}, \tag{10}$$

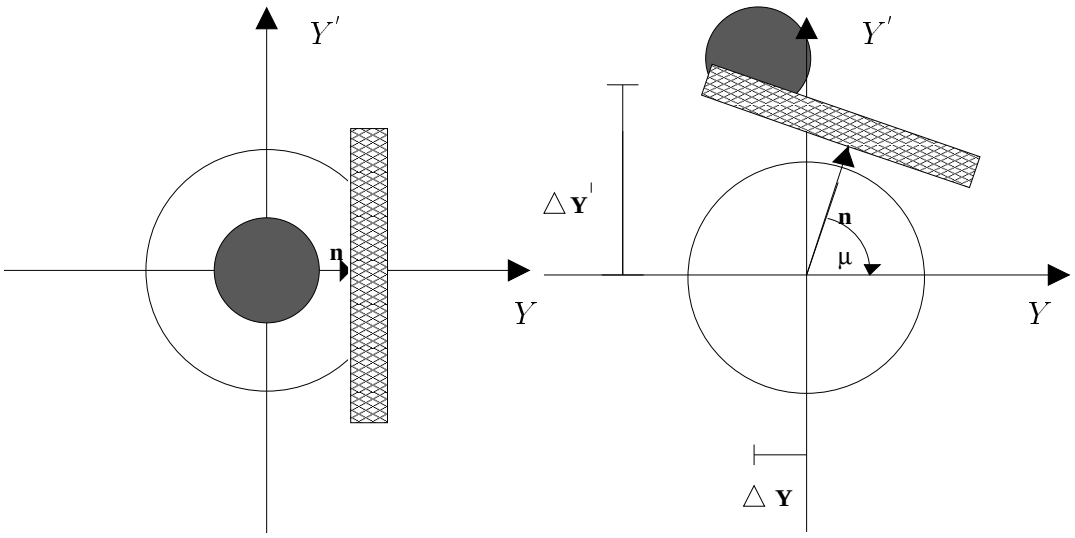

Figure 3:
Left: The TDI collimator in the normalised vertical phase space. The vertical amplitude of the collimator is given by n.
Right: The TDI collimator rotated counter-clockwise by the vertical phase advance between kicker and TDI (μ).

where y and $y^{'}$ are the vertical coordinates, α_y and β_y are the vertical twiss functions and σ_y the vertical r.m.s. beam size. The transfer matrix transporting a particle from one position in the ring to the next is then simply a rotation

$$M(\mu) = \begin{pmatrix} \cos\mu & \sin\mu \\ -\sin\mu & \cos\mu \end{pmatrix} \tag{11}$$

where μ is the vertical phase advance between the two points. The left-hand side of Fig. 3 schematically shows the TDI absorber and a circulating beam in the normalised vertical phase space. The large circle indicates the aperture of the cold magnets. We estimate the required vertical phase advance between kicker and TDI by rotating the TDI collimator in the normalised phase space counter-clockwise until the TDI absorber fully overlaps with the miskicked beam. The right-hand side of Fig. 3 shows the rotated TDI together with the miskicked beam in the normalised phase space. The aperture of the TDI is constrained by the collimation system. In order not to scatter secondary particles into the detector and the cold magnets, the transverse position of the TDI absorber must be larger than the position of the secondary collimator. The recommended positions of the primary and secondary collimators are $n_1 = 7.0$ and $n_2 = 8.2$ respectively [3]. In order to incorporate orbit and optics changes due to dynamic effects during the injection process[2] we assume $n_{TDI} = 9.0$ for the TDI absorber. For the aperture of the cold

[2]The orbit errors change the effective position of the TDI and the optic errors the beam size of the beam ($\sigma = \sqrt{\epsilon \cdot \beta}$). For a vertical β-function of 40 m an orbit error of 0.5 mm corresponds to a change of 1 σ in the normalised aperture of the TDI. A change of the β-function by 10 % corresponds to a change of approximately 5 % in the normalised aperture. Thus, assuming that the closed orbit can change by up to 0.25 mm during the injection process (without an orbit feedback system) and the β-function by up to 5 %, the normalised transverse aperture of the TDI can not be adjusted with an accuracy better than $\pm 0.73\,\sigma$. Hence, we assume $n_{TDI} \geq 9.0$.

elements in the arc we assume $n_\sigma = 9.8$, which is the smallest aperture still compatible with the recommended positions of the collimation system [1]. With n_{TDI} and n_σ being determined by the collimation system, we can express the maximum beam size for which the TDI can protect the cold elements as a function of the vertical phase advance between MKI and TDI. From the right-hand side of Fig. 3 we get

$$m = \sin\mu \cdot \triangle Y^{'} - \cos\mu \cdot \triangle Y - n_{TDI}, \tag{12}$$

where $m \cdot \sigma$ is the size of the miskicked beam.

7 Potential Failure Sources

Introducing orbit and optics errors into Equation (10) the total injection error in normalised coordinates is given by (contributions up to first order in the errors)

$$\begin{aligned} \triangle Y &= \frac{\triangle y}{\sigma_y} \\ \triangle Y^{'} &= \frac{\alpha_y \cdot \triangle y}{\sigma_y} + \frac{\beta_y \cdot \triangle y^{'}}{\sigma_y} + \frac{\beta_y \cdot \triangle \delta_{\theta,nom}}{\sigma_y}, \end{aligned} \tag{13}$$

where α_y and β_y are the average vertical optics function inside the MKI, $\delta_{\theta,nom}$ the nominal kick strength of the MKI, $\triangle y$ a vertical orbit error at the MKI, $\triangle y^{'}$ an error in the trajectory slope, $\triangle \delta_{\theta,nom}$ an error in the kick amplitude and σ_y the vertical beam size at 450 GeV. Table 14 summarises the relevant parameters at the MKI [4]. It is foreseen to adjust the injection with a

β [m]	α	$\delta_{\theta,nom}$ [mrad]	ϵ [m]	σ [mm]
50	-1.5	-0.85	$7.82 \cdot 10^{-9}$	0.63

Table 14: *Injection parameters.*

pilot bunch which allows a proper correction of any orbit and steering errors. However, injection errors can still occur when changing from the pilot bunch to the full batch. An injection error can be caused by three different types of incidents:

- The miskicked beam experiences a large deflection. This occurs when the injection kicker does not fire during the injection or when the circulating beam experiences the nominal injection kick.
- The miskicked beam covers a range of different amplitudes. This can be caused by a timing error for the injected beam or by a miskick of the circulating beam when the miskicked beam passes the injection kicker during its rise or fall time.
- The miskicked injected beam is kicked onto the aperture of the cold magnets. This can be caused by steering errors in the transfer line or by amplitude errors in the injection kicker.

In all cases, the trajectory of the miskicked beam diverges from the nominal closed orbit and particles can reach the cold elements down-stream from the MKI if the particles are not absorbed by the TDI. We discuss each case separately.

7.1 Large Deflections

A large deflection of the beam can be caused either by the absence of the injection kick for the injected beam or by an accidental firing of the kicker while the circulating beam passes the MKI. Neglecting the orbit and optics errors at the kicker, and inserting the nominal kick from Tables 14 into Equation (13) we get a maximum normalised displacement of 67 σ. Such a large offset lies well outside the aperture of the cold elements and all particles of the miskicked beam can easily be absorbed by the TDI absorber. Inserting a $\triangle Y^{'} = 67$ into Equation (12) and assuming, for example, a beam core of 10 σ we obtain a minimum vertical phase advance of 15° between MKI and TDI. No effort has to be made to optimise the vertical phase advance between MKI and TDI in this case.

7.2 Variable Beam Deflection

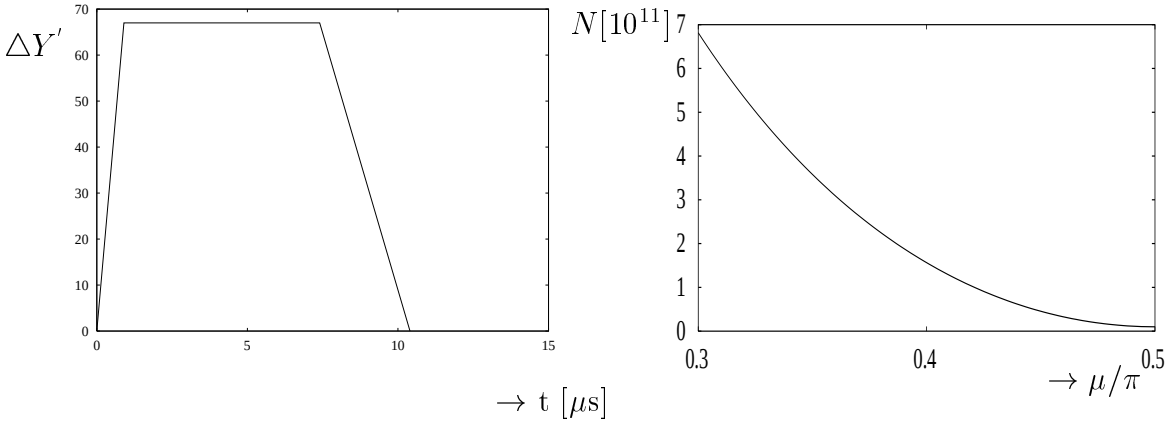

Figure 4:
Left: The kicker pulse for the MKI.
Right: The number of particles which are not absorbed by the TDI as a function of the phase advance between MKI and TDI for $N_b = 10^{11}$, $\beta_{MKI} = 50$ *m and* $\delta_\theta = 0.85$ *mrad assuming that the particles of the miskicked bunches are uniformly distributed in the vertical direction.*

If a beam passes the MKI during its 0.9 μs rise or 3 μs fall time it will experience a displacement which is smaller than 67 σ. The left-hand side of Fig. 4 schematically shows the kicker pulse of the MKI. Approximately 36 bunches can pass the MKI during its rise time and approximately 120 bunches during its fall time. Assuming that the particles of these 156 bunches are uniformly distributed in the vertical direction and neglecting again the orbit and optics errors at the MKI we get from Equation (13) and Equation (12)

$$N_{loss} = \left(\frac{1}{\sin \mu} - 1 \right) \cdot \frac{156 \cdot N_b \cdot (n_{TDI} + m) \cdot \sqrt{\epsilon}}{\sqrt{\beta_y} \cdot \delta_\theta}, \tag{14}$$

where N_b is the number of particles per bunch. The right-hand side of Fig. 4 shows the number of particles which are not absorbed by the TDI as a function of the phase advance between MKI and TDI for $N_b = 10^{11}$, $\beta = 50$ m and $\delta_\theta = 0.85$ mrad. One clearly recognises that a

phase advance of 90° between MKI and TDI gives an optimum protection of the cold elements. However, when evaluating the efficiency of the TDI we must allow for a β-beating of up to 20 % in the real machine. In this case, the phase advance between MKI and TDI can also change by 20 %. Taking the data from the right-hand side of Fig. 4 and reducing the vertical phase advance from the optimum value of $\mu = 90°$ to $\mu = 72°$ yields a particle loss of

$$N_{loss} \approx 2.0 \cdot 10^{11}. \tag{15}$$

In other words, even for the optimum phase advance of 90° between MKI and TDI, one expects losses of up to $2.0 \cdot 10^{11}$ inside the cold magnets. Using the same line of argument and taking a design value of $\mu = 80°$ results in potential particle losses of up to $3.4 \cdot 10^{11}$. For $\mu = 70°$ the particle loss increases to up to $6.8 \cdot 10^{11}$. Furthermore, the number of lost particles increases with decreasing vertical β-function at the TDI. A reduction of 20 % in the β-function at the MKI leads approximately to an increase of 10 % in the number of lost protons.

Determining the minimum required phase advance between MKI and TDI depends on whether the TDI must merely protect the cold magnets from destruction or whether it must also protect the magnets from a quench. The minimum particle loss in Equation (15) is clearly large as compared to the quench limit of approximately $1.0 \cdot 10^9$ protons per unit length (see Appendix B). Furthermore, even for $\mu = 90°$ and a perfect alignment of the TDI absorber the number of backscattered particles from the TDI is of the same order of magnitude as the quench level of the super conducting magnets. It is therefore unlikely that the TDI can protect the cold elements from a quench.

Permanent damage of the magnets can occur for losses larger than $N_{b,crit} = 2.0 \cdot 10^{12}$ or approximately the intensity of 20 bunches (see Appendix A). In this case, even a nominal vertical phase advance of $\mu = 70°$ is sufficient to protect the magnets (including the effect of an additional β-beat of 20 %).

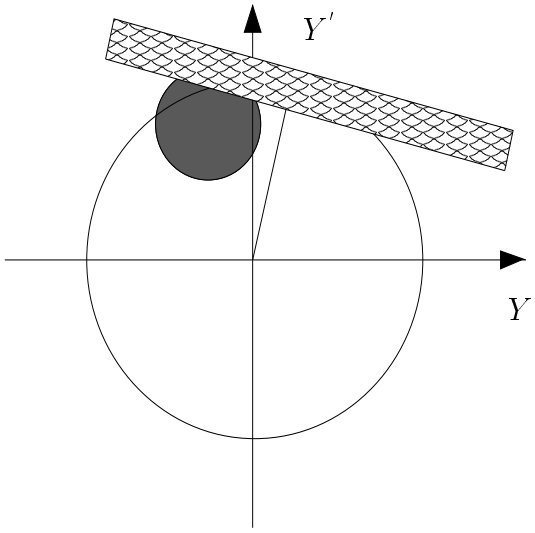

Figure 5:
The TDI in normalised phase space rotated counter clock wise by 75°. The miskicked beam just reaches the aperture of the cold magnets indicated by the outer circle.

7.3 Small Deflections

The most critical situation occurs if a full injection batch falls right on the aperture of the cold elements. This situation is depicted in Fig. 5. For an injection batch of 243 bunches the loss limit given by the magnet protection corresponds to only 8 % of the batch intensity. In the following, we look at two different failure modes:

- Orbit errors (orbit and slope of the injected beam). Can be caused by a faulty ejection in the SPS, energy error in the SPS, magnet errors in the transfer line or faulty injection settings.
- Kick strength. Can be caused by faulty injection settings.

The injection will be optimised with a small intensity pilot bunch and we assume that all static orbit errors and the required injection kick are corrected during this initial setup. Thus, we are only concerned with changes that occur between different injection batches or when changing from the pilot bunch to the full batch injection.

For an orbit error of

$$\begin{aligned} \triangle y &= \pm 2 \text{ mm} \\ \triangle y^{'} &= \pm 40 \ \mu\text{rad} \end{aligned} \tag{16}$$

we get for the injection error in normalised coordinates

$$\begin{aligned} \triangle Y &= 3.2 \\ \triangle Y^{'} &= 8.0 \\ \rightarrow \sqrt{(\triangle Y)^2 + (\triangle Y^{'})^2} &= 8.6 \end{aligned} \tag{17}$$

which is still smaller than the aperture of the cold magnets ($n_\sigma = 9.8$) and even a beam with a Gaussian distribution cut at $4 \cdot \sigma$ can not cause any damage in the cold magnets. However, increasing the angle error to $\triangle y^{'} = 50$ μrad and assuming a Gaussian beam distribution, approximately 20 % of the injected batch lies outside the aperture of the cold magnets [3]. In this case, the particle loss is higher than the limit given by the magnet protection (a permanent magnet damage can occur for losses of more than $N_{b,crit} = 2.0 \cdot 10^{12}$ particles (see Appendix A)). In order to avoid a permanent damage of the cold magnets in this case, the TDI absorber must absorb at least half of these particles, requiring a vertical phase advance of at least 75° between MKI and TDI. Let us recall at this point that a β-beat of 20 % reduces a nominal phase advance of 90° to 75°. Thus, an orbit error with $\triangle y = 2.0$ mm and $\triangle y^{'} = 50$ μrad is just compatible with a vertical phase advance of 90° between MKI and TDI. If more than 20 % of the miskicked batch lies outside the aperture of the cold magnets the TDI can not provide sufficient protection for the cold magnets. Assuming a Gaussian distribution for the injected batch results in a non-linear dependence of the required vertical phase advance on the orbit errors of the injected batch and rather than determining a required phase advance between MKI and TDI, it seems to be more reasonable to determine the maximum orbit error which still results in tolerable losses even without the TDI protection. Equation (16) gives the upper

[3] Particles which lie within the region enclosed by the aperture of the cold magnets and the TDI circulate inside the vacuum chamber until they are absorbed by the main collimation system.

limits for the orbit errors which are still compatible with a Gaussian beam distribution cut at $4 \cdot \sigma$ and without a TDI absorber.

The orbit errors given in Equation (16) are already at the limit of what can be tolerated in the transfer line. For orbit errors larger than those given in Equation (16) the beam can touch the vacuum chamber of the transfer line [5]. In order to avoid errors larger than those given in Equation (16) it would be desirable to have an interlock which prohibits an injection for larger orbit errors.

Errors in the kick strength are another source for a miskick on to the aperture of the cold elements. Errors in the kick strength are expected to be of the order of a few per mill of the nominal injection kick ($\rightarrow \triangle\delta_\theta \approx 0.001$ mrad) and are too small to produce a miskick onto the aperture of the cold magnets. A miskick of $\triangle Y^{'} = 8.5$ requires a kick error of 0.11 mrad. However, it must be ensured that the kick strength can not be adjusted between different batches or when changing from the pilot bunch injection to the full batch injection.

7.4 Summary

Table 15 summarises the required vertical phase advances between MKI and TDI for different failure modes and different protection levels.

$\triangle\mu_0$ for 1 TDI		
Failure Mode	Damage	Quench
Large Beam Deflection	15°	15°
Variable Beam Deflection	70°	No
Small Beam Deflection	No	No

Table 15: *Single TDI absorber: Required vertical phase advance between MKI and TDI for different injection failure modes and protection levels.*

The absence of the injection kick during the injection of a new batch does not cause any danger for the cold magnets provided the vertical phase advance between MKI and TDI is larger than 15°. A more serious failure mode occurs if the injection kicker fires while the circulating beam passes by and consecutive bunches experience kicks of different amplitudes (equivalent to a timing error of the MKI when the injected batch passes). In this case, a nominal vertical phase advance of more than 70° between MKI and TDI is sufficient to protect the cold magnets from permanent damage. A protection against magnet quench seems not possible with only one TDI (even with a vertical phase advance of 90° between MKI and TDI).

Orbit errors in the injection line, if not properly controlled, can result in injection errors which place the injected batch right on the aperture of the cold magnets. For a Gaussian beam distribution, the required vertical phase advance between MKI and TDI has a non-linear dependence on the orbit errors and rather than determining a required phase advance, it seems to be more reasonable to determine the maximum orbit error which still results in tolerable losses even without the TDI protection: Orbit errors at the end of the beam transfer line must

remain below $\triangle y \leq \pm 2$ mm and $\triangle y^{'} \leq 40$ μrad to avoid a permanent damage. Larger orbit errors must be either prevented or the firing of the injection kicker must be prohibited.

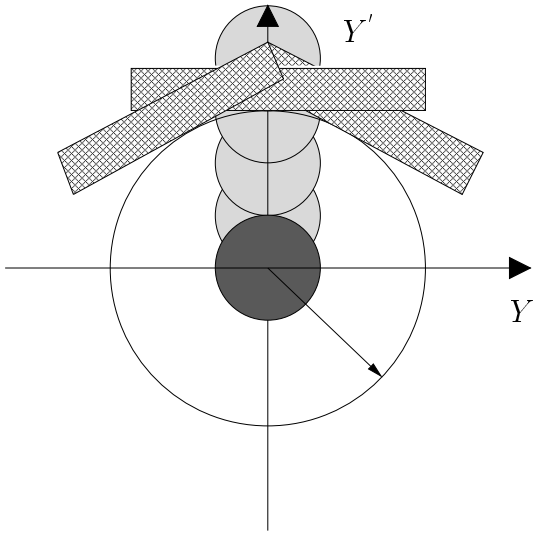

Figure 6:
The TDI and two additional collimators in normalised phase space. The additional collimators stabilise the system against β-beat in the machine.

$\triangle\mu_0$ for 3 TDI's		
Failure Mode	Damage	Quench
Large Beam Deflection	20°	20°
Variable Beam Deflection	70°	90°
Small Beam Deflection	75°	?

Table 16: *More than one TDI absorber: Required vertical phase advance between MKI and the first TDI for different injection failure modes and protection levels.*

The protection potential of the TDI can be improved by introducing additional collimators downstream of the TDI. For example, generating a vertical MKI-TDI phase advance of 75° and introducing two additional collimators with a vertical phase advance of 90° and 105° to the MKI stabilises the system against β-beat in the machine and allows a damage protection even in the case of small beam deflections (see Section 7.3). This scenario is illustrated in Fig.6. The aperture of the TDI must be smaller than the aperture of the cold magnets and larger than the aperture of the secondary collimators of the main collimation system. Thus, the TDI aperture must be in the range $8.2 < n_{TDI} < 9.8$.

Adding a collimator with a 90° phase advance downstream from the TDI allows the absorption of the back-scattered particles from the TDI and can provide a quench protection in case

of a variable beam deflection (see Section 7.2). However, further studies are necessary for fully evaluating such an extended protection system. Table 16 summarises the preliminary estimates for the required vertical phase advances between MKI and TDI for such an expanded system.

8 Conclusion

Using the conservative criterion of a circular aperture the presented study estimates the maximum β-function values compatible with the aperture of the injection elements and the current crossing-angle beam separation scheme during injection. They are summarised in Table 7 and are compatible with the optics solutions for version 5.0. The optics version 5.0 is designed with a vertical phase advance of 90° between MKI and TDI. However, this study shows that one TDI can not provide a protection against magnet quench, and in some cases even magnet damage, for all failure modes of the injection. The study looked at three different classes of failure modes: large beam deflections (e.q. the absence of an injection kick for the injected beam or the full injection kick for the circulating beam), variable beam deflection (e.q. some of the beam passes the MKI during its rise or fall time), small deflections where the full batch reaches an amplitude comparable to the aperture of the cold magnets. In the first case both protection levels (damage and quench protection) can be achieved by one TDI with less than 20° phase advance between MKI and TDI. In the second case, damage protection can be achieved by one TDI with a vertical phase advance of more than 70° between MKI and TDI. But protection against magnet quench is not possible, even for an optimum design value of 90° phase advance between MKI and TDI. In the third case neither damage nor quench protection can be provided by only one TDI. Table 15 summarises the required phase advances between MKI and TDI for the different failure modes and protection levels. Recognising that the maximum protection possible with only one TDI is already reached with a vertical phase advance of 70° between MKI and TDI one can relax the constraints on the optics. For example, lowering the vertical phase advance between MKI and TDI from 90° to 80° allows the construction of anti-symmetric optics solutions with $\beta_x^* = \beta_y^*$ and $\alpha_x^* = 0.0 = \alpha_y^*$ at the IP. A phase advance of 90° between MKI and TDI requires different optics solutions for Beam-1 and Beam-2.

Aiming for a better protection of the cold magnets (damage and quench protection for all injection failure modes) requires to complement the TDI with collimators and a tight control of the orbit errors in the beam transfer line and the TDI during injection. However, more studies are required for such a scenario. The LHC optics version 6 will be designed with a MKI-TDI phase advance of 80° with provision to reach 90° if further studies show it to be necessary. In collaboration with the BT experts, the critical cases will be reviewed.

References

[1] J.B. Jeanneret and R. Ostojic, 'Geometrical acceptance in the LHC Version 5.0', LHC Project Note 111, September 1997.

[2] J.B. Jeanneret, 'Constraints for the injection straight sections in the LHC' LHC Project Note 40, March 1996.

[3] Minutes of the 11^{th} meeting of the Parameter and Layout Committee, P. Lefevre, revised version, 9. September 1996.

[4] O. Brüning, LHC Project Note 142, May 1998.

[5] A. Hilaire, private communication, April 1998.

[6] P. Sievers, Lab II/BT/74-2, June 1974.

[7] A. Ijspeert, private communication, February 1998.

[8] D. Leroy, private communication, February 1998.

[9] Cryogenie, ses applications en supraconductivite, Institut international du Froid,1995.

[10] J.B.Jeanneret et al, CERN LHC project report 44,1996.

[11] E. Weisse, private communication, October 1997.

[12] T. Trenkler et J.B. Jeanneret, CERN SL/Note 94-105(AP),1994.

[13] N. Catalan et al., CERN LHC project report 156,1997.

[14] J.B.Jeanneret et al, CERN LHC project report 44,1996.

A Damage of a s.c. cable by fast heat deposition

In the case of fast, or adiabatic deposition of heat in the cable, we can consider that by inertia the cable has no time to expand [6]. It is then under longitudinal stress, with a pressure

$$\Delta p = E\frac{\Delta l}{l} \tag{18}$$

with E the elastic modulus and $\Delta l/l$ the relative elongation of an elemnt which is not under stress. The critical stress Δp_c is the elastic limit of copper, or $\Delta p_c \approx 50$ Nmm^{-2} [7][8]. Both the NbTi and the insulator have a better critical limit. Using $E = 1.3\ 10^5$ Nmm^{-2} we get the critical elongation from (18)

$$(\frac{\Delta l}{l})_c \approx 3.85\ 10^{-4}. \tag{19}$$

The thermal elongation at low temperature is not linear with the temperature T. We get a good fit of existing data [9] with

$$\frac{\Delta l}{l} = aT^3 + bT^4 = -1.121\ 10^{-12}T^3 + 4.605\ 10^{-10}T^4. \tag{20}$$

The temperature T_c at which the critical elongation is reached is obtained by solving

$$aT^3 + bT^4 - (\frac{\Delta l}{l})_c = 0 \tag{21}$$

Finally the relation between the temperature and the heat deposition is given by the Debye law

$$\Delta Q = 9RT\frac{\rho}{m_A}(\frac{T}{\Theta_D})^3 \int_0^{\frac{\Theta_D}{T}} \frac{z^3 dz}{\exp(z) - 1} \tag{22}$$

which has no primitive. For copper, the temperature of Debye is $\Theta_D = 340$ K, $m_A = 65.5$ g and $\rho = 8.96$ gcm^{-3}, while $R = 8.3$ JK^{-1}(mole)$^{-1}$.

The equation (21) solves with $T_c = 104$ K. The critical energy deposition per unit volume is obtained by integrating numerically (22) between $T = 0$ and $T = T_c$, or

$$\Delta Q_c = 87 \text{ Jcm}^{-3}. \tag{23}$$

A slightly larger effective heat reserve (40%) might be used [10] if the presence of NbTi in the cable is taken into account (the wires are made of 38% of NbTi and 62% of Copper). But in the abscence of a good estimator for the transverse diffusion of heat at the nanosecond time-scale, it is safer to use the copper limit.

The maximum density of energy deposition per proton touching the beam screen is $\epsilon_{inj} = 3.8\ 10^{-11}$ Jcm^{-3} at injection (450 GeV/c) and $\epsilon_{top} = 1.3\ 10^{-9}$ Jcm^{-3} at top energy (7000 GeV/c) [10]. The limit of damage is therefore reached when the number of protons lost at one location exceeds $n_c = \Delta Q_c/\epsilon$, or

$$n_c^{inj} = 2.3\ 10^{12} \text{ protons} \tag{24}$$

$$n_c^{top} = 6.7\ 10^{10} \text{ protons} \tag{25}$$

Using a bunch intensity of $n = 10^{11}$ protons, the critical number of bunches would be respectively

$$n_b^{inj} = 23 \text{ bunches} \tag{26}$$

$$n_c^{top} = 0.7 \text{ bunch} \tag{27}$$

The adiabaticity of the process for 23 bunches is justified by comparing the time for the stress wave to propagate at the speed of sound $v_{sound} \approx 2000$ ms^{-1} in the NbTi/Cu compound [8] over the length of a shower $l \approx 1$ m [10], i.e. $\Delta t = l/v_{sound} = 5\ 10^{-4}$ s to the duration of a train of 23 bunches $\delta t = 23 \cdot 25\ 10^{-9} \approx 6\ 10^{-7}$ s.

B Scattering out of the TDI

Some energy can leak out of the TDI in two ways.

If the MKI do not work during an injection, the entire batch falls on the TDI at a distance of ≈ 30 mm from its inner edge (the 'impact parameter'). No substantial energy is scattered by the inner face back into the acceptance of the ring, but a diffuse halo of low energy particles escapes by the rear side of the TDI. The power deposition on the head of the coil of the D1 magnet was computed with the Fluka program [11]and was found comparable to but larger than the quench level in this magnet [11].

In the case of a random trigger of the MKI, the beam is sprayed in a continuous way during both the rising and the falling edge of the MKI kick, in addition to correctly ejecting the fraction of the beam in phase with the flat top ≈ 40 mm away from the beam axis on the TDI. At the TDI, the distance between two sprayed bunches is

$$\delta y = L_{mki-tdi} \Delta\Theta_{mki} \frac{\delta t}{\tau_1 + \tau_2} = 0.3 \text{ mm} \tag{28}$$

with $L_{mki-tdi} \approx 60$ m the distance between the TDI and the MKI, $\Delta\Theta_{mki} = 0.8$ mrad the full kicker strength, $\tau_1 = 10^{-6}$ s the rise time of the kicker, $\tau_2 = 10^{-6}$ s its fall time and $\delta t = 25 \cdot 10^{-9}$ s the distance between two bunches. With a bunch intensity of $n_b = 10^{11}$ and a transverse size of $dy \approx 2$ mm, the density of protons falling at the edge of the TDI is therefore quite uniform and equal to

$$\frac{dn}{dy} = 3.3 \cdot 10^{11} \text{ protons/mm} \tag{29}$$

The scattering at the edge of the TDI is simulated by a single-jaw version of the K2 program [12][13]. The distribution of impact parameters is made uniform while the angular distribution is fixed to a single value Θ_{in}. The angle Θ_{in} is varied from one run to the other to evaluate the effect of the relative misalignment of the miskicked beam with the inner face of the TDI. A notional misalignment is $\delta\Theta_{al} = \sqrt{2}\delta_{al}/L_{tdi} = 1.4 \cdot 10^{-4}$ rad with $\delta_{al} = 0.5$ mm being the variance of the misalignment of the TDI and $L_{tdi} = 4$ m its length. This value can be compared to the divergence of the miskicked beam at the surface of the TDI, either $\Theta_{div} = \sigma_{tdi} \approx 10^{-5}$ mrad and to the betatronic divergence, or $\Theta_{beta} = -(\alpha_{tdi}/beta_{tdi})\sigma_{tdi} \approx 10^{-5}$ mrad where $\sigma_{tdi} = \sqrt{\varepsilon\beta_{tdi}} \approx 1$ mm with $\beta_{tdi} \approx 100$ m and considering a beam of transverse size $3\sigma_{tdi}$.

Θ_{in} [mrad2]	Δn for $\Delta\mu = 90^o$	Δn for $\Delta\mu = 60^o$
$-2 \cdot 10^{-4}$	$8.6 \cdot 10^9$	$20.0 \cdot 10^9$
$-1 \cdot 10^{-4}$	$4.7 \cdot 10^9$	$10.0 \cdot 10^9$
0	$0.7 \cdot 10^9$	$0.7 \cdot 10^9$
$1 \cdot 10^{-4}$	$2.7 \cdot 10^9$	$6.7 \cdot 10^9$
$2 \cdot 10^{-4}$	$5.3 \cdot 10^9$	$11.2 \cdot 10^9$

Table 17: Rate of protons scattered out of the TDI in the range of normalised amplitudes $9.5 < A < 10.5$ for different conditions of alignment.

The distribution of the normalised amplitudes of the protons scattered off the TDI dn/dA is built by computing the normalised variables approximated by the suppression of the α-dependent term, which depends on a particular optics but is also negligeable (see above), as follows

$$X = \frac{x}{\sigma_x} \qquad X' = \frac{x'}{\sigma_x}\beta_x \tag{30}$$

$$Y = \frac{y}{\sigma_y} \qquad Y' = \frac{y' - \Theta_{in}}{\sigma_y}\beta_y + A_{tdi}\sqrt{\frac{1}{\sin^2 \Delta\mu} - 1} \tag{31}$$

with x, x', y, y' the transverse coordinates in the reference system of the TDI, where the longitudinal coordinate is parallel to the inner face of the jaw, $A_{tdi} = 9.5$ the normalised aperture of the TDI and $\Delta\mu$ the phase advance between the MKI and the TDI. For every protons which is not absorbed, the quantity $A = \sqrt{X^2 + X'^2 + Y^2 + Y'^2}$ is stored in an histogram. The density of protons of amplitudes in the range $9.5 < A < 10.5$ integrated from the histograms is given in Table B for different Θ_{in} and for $\Delta\mu = \pi/2$. The range of amplitude A corresponds approximately to a local default of alignment, where most of the corresponding protons might impact. The quench level for fast transient losses is $\Delta n_q = 10^9$ p/m [14]. It can be concluded that depending on the relative misalignment of the beam and the TDI a quench is likely to occur even at the optimum phase advance.

Using a phase advance of $\Delta\mu = 60^o$ the rate of losses is larger by a factor 2-3, and the number of additional uncaptured bunches is $\delta n_b = (1/\Delta\mu - 1)\sigma_y/\delta y = 2.7$ bunches, a value 10 times smaller than the limit of permanent damage obtained in Appendix A.